Partial Discharge Investigation of Form-Wound Electric Machine Winding for Electric Aircraft Propulsion

Yalin Wang, *Member, IEEE*, Thanatheepan Balachandran, Yovahn Hoole, Yi Yin, *Member, IEEE*, and Kiruba Sivasubramaniam Haran, *Fellow, IEEE*

Abstract—**Electric machine for aircraft propulsion is required to have high power density and high reliability, but the harsh operating environment, such as low air pressure, will challenge the motor's insulation system. This article presents the partial discharge (PD) investigation of the form-wound winding in high-frequency electric machines for electric aircraft propulsion. Experimental results show that the PD activity is largely enhanced due to the decrease in air pressure. PD inception voltage (PDIV) decreases to ∼50%–60%, and the PD magnitude dramatically increases when the pressure drops from 1 to 0.2 atm. Several windings with introduced defects were also tested to extract features from phase-resolved PD (PRPD) analysis, which can be used for PD pattern recognition. In addition, a PD-based failure precursor, combining the apparent charge, number, and phase interval of the monitored PD profile, is proposed to monitor the insulating condition of the thermally and electrically aged windings. The proposed failure precursor generally shows a rising trend with the aging time in this article. The application of the proposed failure precursor on online condition monitoring needs more investigation through long-term online observation of the electric machine.**

Index Terms—**Electric aircraft, electric machine, form-wound winding, partial discharge (PD).**

I. INTRODUCTION

ELECTRIC aircraft attracts increasing attention because the conventional nonelectrical system will be replaced by the more electrical system to improve efficiency, and to reduce weight, fuel cost, and carbon emission [1]–[3]. A number of companies have already developed one- or two-passenger electric aircraft for short flights, as well as electric hybrids that could travel hundreds of miles. High-speed electric machines have the opportunity to be widely used for electric aircraft propulsion in the future [4]. The most challenging part of electric propulsion lies in the high specific-power requirement and long-time reliability of the electric machine, especially when it operates at high-voltage and low-pressure conditions. The electric machine on an aircraft may experience 0.2-atm air pressure at a cruising altitude of 11.9 km [5], which will pose huge threats to the stator winding insulation. According to surveys, stator faults generally account for 66% of the total machine failures for high-voltage electric machines [6].

Partial discharge (PD) has been widely acknowledged to be an effective and feasible indicator for the offline evaluation and online condition monitoring of an electric machine's insulation [7]. Research shows that PD is sensitive to problems associated with overheated insulation, loose stator bars, and pollution, all of which can cause in-service failures with long associated outages and high-cost repair [8]. Analysis based on the processing of PD signals, such as PD pattern recognition, has applications as discriminating the PD source and possible location, evaluating insulation condition, and preventing complete failure [9], [10]. Since the electric machine for aircraft propulsion will inevitably operate under high altitude conditions, the effect of low air pressure on PD magnitude, phase distribution, and insulation degradation needs profound exploration. PD measurement of twisted pairs of winding coil shows that the insulation is dramatically degraded with the decrease in pressure due to the PD [11]. It is also found that the lower pressure environment results in a decrease in inception voltage and a marked increase in maximum PD magnitude [12]. In [13], PD of polyimide films was investigated at various pressures, temperatures, and humidity levels. It shows that the lifetime of the insulation with varying temperatures and pressure seems to increase as the dissipated energy decreased. However, the PD test of form-wound windings at low air pressure and the variation of PD activities of typical defects in these windings have not been fully investigated.

In a National Aeronautics and Space Administration (NASA) project, a 1-MW high-frequency permanent magnet synchronous machine (PMSM) was proposed by our team to achieve 13-kW/kg specific power to enable hybrid-electric

aircraft propulsion [14]. Air-gap litz wire windings were fabricated. The development and design details of this winding considering the electric losses, dielectric capabilities, heat dissipation, and mechanical forces are presented in [15]. This article presents the possible PD challenges to the insulation of these form-wound windings when they are used for electric aircraft propulsion. The form-wound windings and those with four typical insulation defects, which represent the general causes of stator insulation failure, are electrically pressed under various pressures. The PD inception voltage (PDIV) and PD patterns are analyzed to investigate the PD vulnerability and fault-type recognition of these windings. In addition, the normal winding, which does not have human-introduced defects and has been checked for insulation integrity by insulation resistance measurement, is thermally and electrically aged. A PD-based failure precursor, combining the apparent charge, number, and phase interval of the monitored PD profile, is proposed to monitor the insulating condition. Hopefully, this article may provide insight and useful suggestions to reliable stator insulation design for electric aircraft propulsion.

II. MOTOR DESIGN AND WINDING INSULATION STRUCTURE

Increasing the specific power of electrical machines is a critical step toward more electric aircraft. This involves decreasing weight by minimizing iron and increasing power by raising the machine's operating frequency. When designing the machine and the winding insulation, electrical loss, mechanical considerations, heat dissipation, and dielectric capabilities are considered. A 20-pole, slot-less structure is proposed to reduce the high-frequency iron loss and stator yoke weight. The cutaway diagram and cross section of the full motor are shown in Fig. 1(a) and (b). Type 8 litz wire with a rectangular shape formed by 15 bundles was chosen to reduce the ac losses. Each bundle encases 44 copper strands of size 38 American wire gauge. Each winding includes three overlapping litz wire turns. According to the thermal analysis of this motor and considering the effect of cooling method [16], the Duralco 128 class H (180 °C rated temperature) resin is applied between the three turns and covers the surface of the three turns to provide structural integrity, enhance insulation, and improve radial thermal conductivity. Glass fiber cloth wraps each turn for added insulation redundancy. The windings are attached to the stator metal yoke with 0.2-mm Duralco 128 resin, as shown in Fig. 2. A summary of stator parameters is shown in Table I.

Generally, stator winding insulation is a laminated system consisting of numerous layers of mica paper tape on a fiberglass backing material impregnated and consolidated with a synthetic resin, usually epoxy or polyester-based [17]. Voids or delaminations in the groundwall insulation of stator windings are common defects and result from the manufacturing process and/or operating stresses. The high energy discharge will cause the erosion of the void walls and result in the growth of the delamination and potentially failure in the long term. In addition, end-winding areas of rotating machines are prone to environmental contamination and mechanical abrasion. The
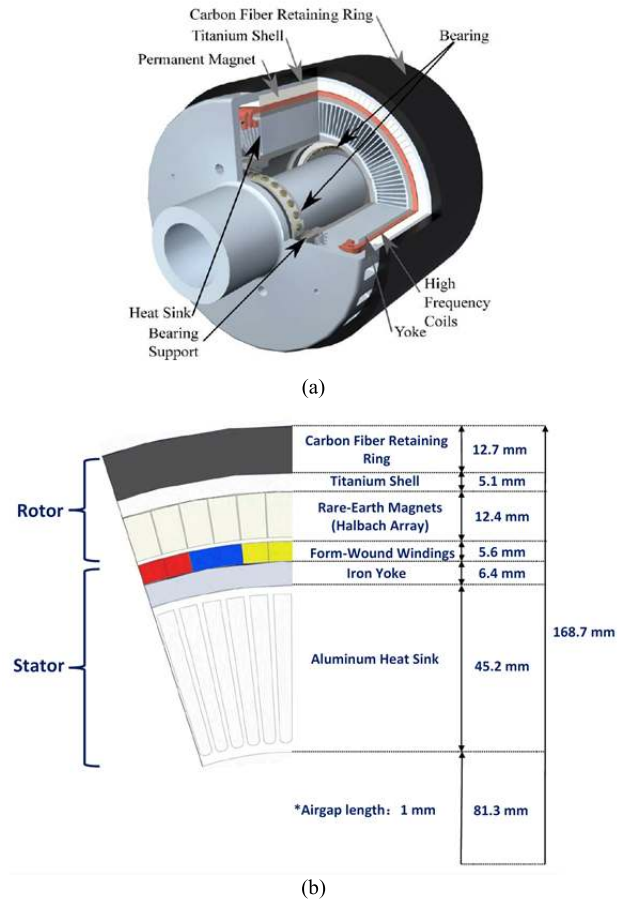

Fig. 1. Designed motor for electric aircraft propulsion. (a) Cutaway diagram (b) Cross section.

TABLE I
STATOR DESCRIPTION

Metric	Value
Winding Active Length	224 ± 3mm
Pole Pairs	10
Phases	3
Weight	37.6 ± 1 kg
Rated Total Current	930 A$_{rms}$
Rated Line Voltage	650 V$_{rms}$
Rated Temperature	180 °C
Frequency	2.5 kHz
Insulation Class	H

surface of the end winding may deteriorate by contaminants, such as salt, cement dust, lubricating oil, and brake dust [17]. This deterioration can distort the electrical field in the end winding and lead to corona and surface tracking, and eventually cause phase-to-ground and phase-to-phase failure of the machine. The end winding area usually is the position where the electric field is concentrated. If the electric stress in groundwall voids or air gaps exceeds breakdown strength, PD will occur and will eventually erode a hole through the groundwall causing phase-to-ground failure [18].

The typical defects in stator windings are elaborated in several standards, such as IEC 60034-27-1 and IEC 60034-27-2 [19], [20]. Based on these standards and considering the
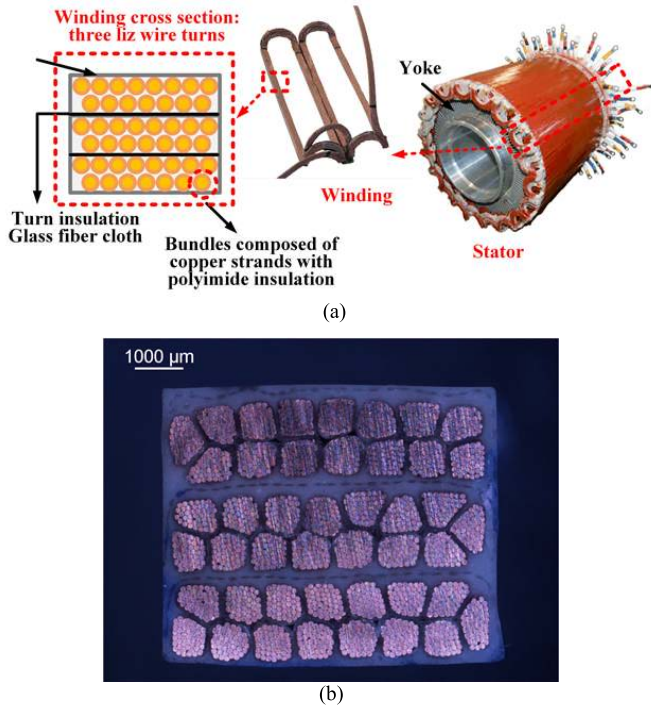
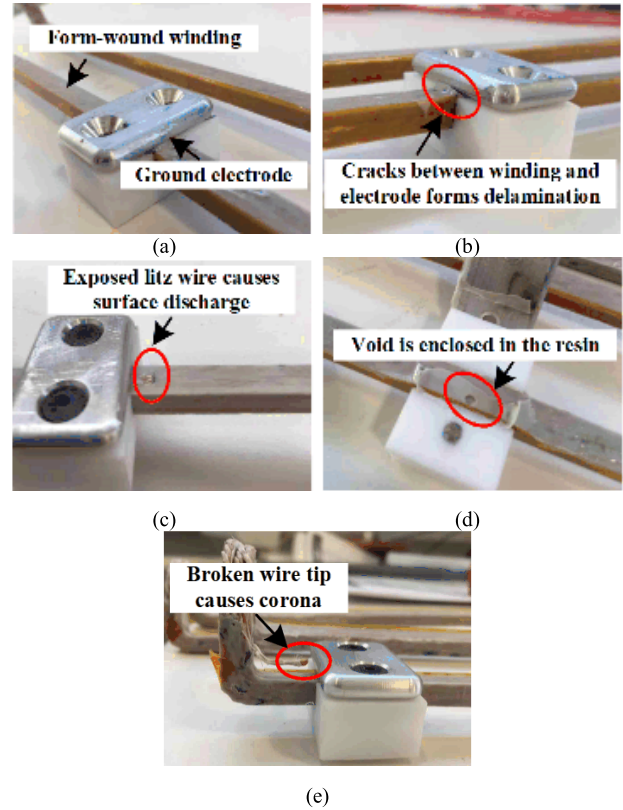Fig. 2. Winding insulation structure. (a) Winding and stator. (b) Cross section of a completed winding.

Fig. 3. Photographs of the defect samples and the normal winding. (a) Normal winding. (b) Delamination. (c) Surface defect. (d) Void defect. (e) Corona defect.

particular structure of our air-core form-wound windings, the normal winding and the windings with four kinds of defects (delamination, surface, void, and corona defect) were fabricated, as shown in Fig. 3(a)–(e). It should be noted that these four types of defects are not identical to those recommended in IEC standards due to the special structure of this motor. Therefore, PD patterns of these four defects are not the same to those in IEC standards, which means that combined patterns may appear, especially when the PD activity is dramatically enhanced at low air pressure.

The normal winding was checked by an insulation resistance measurement to have more than 50 GΩ under 1-kV dc high voltage. Therefore, the normal winding is assumed to be a healthy winding. A ground aluminum plate/electrode with 20 × 30 × 5-mm size and a Teflon block with a square trench were properly set to fix windings and form different types of defects. For the normal winding, the ground electrode was attached to the winding surface with 0.2-mm-thick Duralco 128 resin and screwed tightly on the Teflon block via two fixed holes. This setup aims to simulate the situation of the real stator winding shown in Fig. 1. The trench of the block is 0.2 mm deeper than the winding, so that the attached resin can be controlled to this thickness when the flat ground electrode is firmly fixed on the block. Regarding the delamination windings, cracks were introduced between the winding and the ground electrode by tearing the cured ground electrode apart from the winding. The winding was clamped tightly by the electrode and Teflon block with screws. This is to simulate the detachment of the winding from metal yoke, because the temperature gradient and coefficient of thermal expansion difference between the metal yoke and windings

are significant. Cracks can appear between the metal yoke and windings with long-term operation and temperature cycling. For the surface defect winding, the copper conductor of the uppermost turn was exposed with a 1-mm × 2-mm area in the middle, and the electrode was horizontally 2 mm from the exposed area edge. The void defect is made by injecting 1-mL air with a syringe into the resin between winding and ground electrode during the curing process. The major air bubbles are enclosed in the insulation, which agrees with the common void setup in the literature. Note that the bubbles may spread and be exposed to the outside air, which is the situation in real manufacturing. For the corona defect, a strand of litz wire in the end-winding area was broken and has a loose end pointing at the ground yoke 2 mm away. The electric field around the wire tip is concentrated to cause the corona. The structures of these defect samples were verified by the electrostatic field simulation to have electric field concentration around the defect position, so that the PD will occur at these positions rather than those with inherent defects in the winding.

III. EXPERIMENT SETUP AND PROCEDURE

A PD test system is built, as shown in Fig. 4. Test samples are put into a vacuum chamber and electrically stressed by the combination of a linear power supply and a power transformer. The pressure in the chamber is controlled by a vacuum pump. The temperature of the winding is controlled by a temperature controller and a ceramic heating pad fixed on the ground
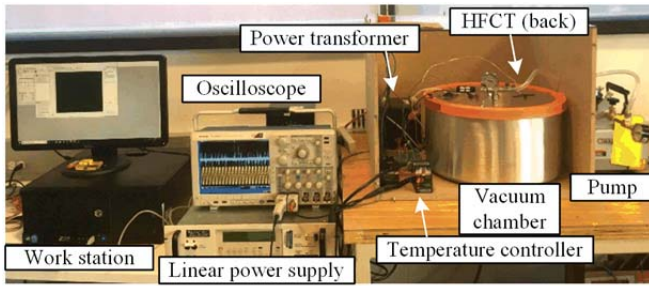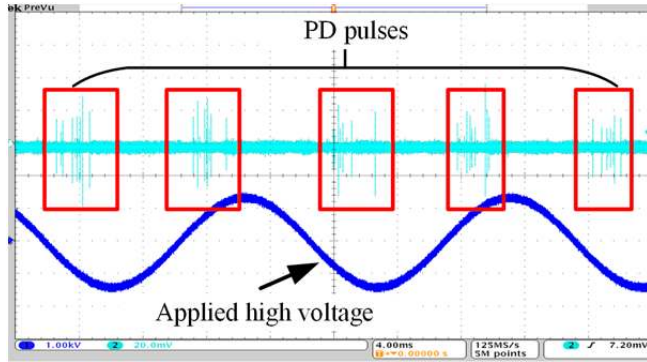
Fig. 4.   Photo of the PD test bench.

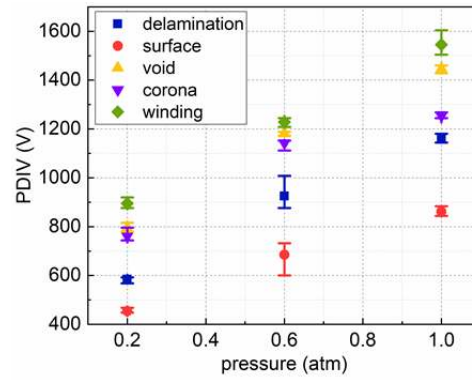Fig. 5.   Typical PD signal obtained by the PD test bench.

Fig. 6.   PDIV of all four defect samples and the normal winding at room temperature various pressures.

The applied voltage linearly increases until PD occurs to obtain the PDIV. The PD patterns are acquired under constant applied voltage for all the samples. The sampling starts once the voltage is applied.

2) PDs of the normal windings were measured during an accelerated aging condition to investigate the PD trend and propose the failure precursor. The accelerated aging setup is based on IEC 60034-18-33 standard [23], which gives the guidelines for simultaneous electrical and thermal aging. A 2200–2800-V_{rms} 60-Hz sinusoidal voltage and 240 ° were applied to the windings to achieve reasonable failure timescale. The PD signals were recorded until failure, and the experiment follows the IEC 60034-27-1 [19] and IEC 60034-18-42 [24] standards.

IV. EXPERIMENTAL RESULTS AND DISCUSSION

The PDIV and PD magnitude and phase distribution of the normal winding and windings with defects are analyzed to provide PD-free design suggestions and PD pattern recognition for discriminating the PD source and possible location, respectively. In addition, several features are extracted and synthesized as a failure precursor from the PD profile based on the thermal and electrical accelerated aging results.

A. PDIV

According to IEC 60270, PDIV is defined as the applied voltage at which repetitive PDs are first observed in the test object when the voltage applied to the object is gradually increased from a lower value at which no PD is observed. The PDIV of all four defect samples and the normal winding at various pressures are shown in Fig. 6. Each defect sample was tested ten times at each pressure. The normal winding has the highest PDIV value in all samples, whereas the surface defect has the lowest PDIV value. It should be noted that the PDIV value is related to the setup of the defect samples, such as the distance between the wire tip and ground electrode for corona sample. The results indicate that the introduction of defects to the form-wound winding decreases the PDIV to some extent, which is reasonable and agrees with general understanding. In order to compare the degree of PDIV reduction of these samples with pressure, the normalization is performed and

electrode. A high-frequency current transformer (HFCT) with a frequency range of 10 kHz–400 MHz surrounds ground wire to monitor the PD signal. Before testing the samples, the measuring system was calibrated with a pulse generator and by means of an algorithm elaborated in [21] to have 10-pC resolution. In addition, a 6-kV 60-Hz sinusoidal voltage was applied to check against background discharge. Typical measured PD signals are shown in Fig. 5.

It should be noted that due to the EMI issue and the power quality requirement for the airplane specified by standards, such as MIL-STD-704, proper *LC* filters will be set between the electric machine and the driver to eliminate harmonics. According to our simulation results and previous experiments [22], the distortion factor of the applied voltage is around 0.02, which is in compliance with the specification in MIL-STD-704 and makes the waveform almost the perfect sinusoidal waveform. In other words, the machine will be driven by a sinusoidal waveform rather than the general pulse width modulation (PWM) waveform. Therefore, the PD experiments in this article were all performed in sinusoidal voltage. Although the frequency of the applied voltage in this article is less than that of the real case, it can still give similar qualitative PD characteristics and the effect of air pressure is the main focus in this article. We will perform the PD measurement at a higher frequency soon and the results will be presented in the future.

Two sets of experiments were performed as follows.

1) PDs of the four defect samples and the normal winding were tested at room temperature and at 1, 0.6, and 0.2 atm to investigate the effect of air pressure on PDIV and PD patterns.
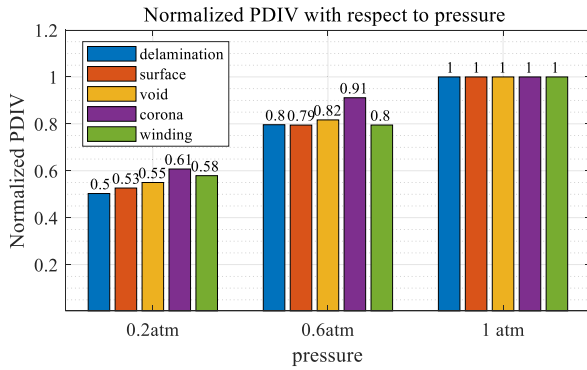
Fig. 7. Normalized PDIV of all four defect samples and the normal winding at room temperature and various pressures.

shown in Fig. 7

$$U_{\text{in}}(P) = \frac{U_i(P)}{U_i(P_0)} \qquad (1)$$

where $U_{\text{in}}(P)$ is the normalized PDIV at pressure P for each kind of defect samples, and $U_i(P_0)$ and $U_i(P)$ are the recorded average PDIV at 1 atm and pressure P for each sample. PDIV decreases with the drop of pressure for all the defect windings and the normal winding. When the pressure drops to 0.2 atm, which is the situation for aircraft at a cruising altitude, the PDIV decreases to approximately 50%–60% of that at 1 atm. The decrease of PDIV can be explained by Paschen's law [25]. The physical mechanism behind this lies in the increase of the mean-free path with the decrease in pressure.

The great reduction of PDIV will impose harm to winding insulation, causing electrical aging at low applied voltage. For example, the windings treated as PD-free at the normal pressure are possible to experience PD when it applied to aircraft at the cruising altitude. Therefore, one should be cautious and consider a 50%–60% margin given the PDIV data at the normal pressure when designing the insulation structure of the machine windings for aircraft propulsion.

B. PD Phase and Magnitude Distribution

PD signals detected by the HFCT are always displayed in pulse form, and they are recorded in relation to the applied sinusoidal ac high voltage. The PD pulses appear at some certain phase angle φ with some certain discharge magnitude or apparent charge Q. It is widely acknowledged that the illustration of PD activity relative to the phase of an ac cycle allows for identifying the discharge root cause, thus the defects can be appropriately handled [26]. Phase-resolved PD (PRPD) is an illustration of the PD phase and magnitude information associated with applied ac voltage by superimposing PD pulses on one ac cycle and counting their number densities or discharge rates in the divided phase angle intervals. The PRPD patterns of the four defect samples and the normal winding at various pressures are composed of PD signals in 20 min, with sampling interval of 1 s, as shown in Fig. 8. It should be noted that the PRPD patterns have been

checked to be time-invariant by comparing the PRPD patterns during the whole 20-min sampling. The reason for choosing 20 min is to obtain denser data and give a better demonstration. The scatter plot is color-coded to denote the number of PD occurrences at a certain phase and magnitude. As can be seen from Fig. 8, the PD magnitude, phase, and their distribution are diverse with respect to defect type and pressure. The PRPD patterns of various defect samples are compared with those from standards and other literature. According to IEC 60034-27-2, the PRPD pattern of the delamination sample will show a less round shape than the void PRPD pattern, and sometimes an almost triangular shape [20]. The delamination PRPD pattern at 1 and 0.6 atm shown in Fig. 8(a) agrees with this description. It is recorded in IEC 60034-27-2 that surface PD in slot shows triangular shape at both positive and negative half cycles. Although the designed windings in this article are air-core form-wound windings, which are attached to the outer surface of yoke rather than inserted in the slot, the detected surface discharge occurs in the air gap between the metal yoke and the side of the winding. This discharge is similar to the slot discharge in terms of the insulation structure and position at which PD occurs. The main characteristic of the internal void PRPD pattern is the symmetry between the positive and negative PDs, combined with a round shape, which coincides with the void PRPD pattern at 1 and 0.6 atm shown in Fig. 8(c). It is found that the void discharge at 0.2 atm has high magnitude PD at the rising of positive half cycle and falling of negative half cycle, which makes the pattern look like "triangle" and surface discharge may occur simultaneously. Regarding the corona defect, corona activity often happens at the stress grading coating position when the field grading system is not adequate, resulting in a high local electrical stress. However, the corona setup in this article is more like a needle-plane corona setup, because there is no stress grading coating for this air-core form-wound winding due to the special insulation structure. According to other literature [27], [28], in general, corona discharges occur in the negative cycle at the peak of the negative half cycle, which is consistent with the pattern shown in Fig. 8(d). At 0.2 atm, the PD magnitude dramatically increases and the PD phase distribution becomes sparse, because the discharge mechanism may change from Townsend avalanche or weak streamer to strong streamer or arc discharge, which may introduce surface discharge. The exact mechanism causing the PRPD pattern change still needs further investigation and will be reported in future papers.

Generally, PD magnitude increases with a decrease in pressure. The reason is that the mean-free path at low air pressure is greater than that at 1 atm, thus the free electrons can obtain higher energy and cause more intense discharge. The PD inception phase angle shifts to the left in both positive and negative half cycles, which can be observed from the movement of the red vertical dotted lines shown in Fig. 8. This phenomenon depends mainly on reduced PDIV values. It is noted that the inception phases of the positive and negative half cycle of the defect samples can shift across 0° and 180° at 0.2 atm, which means PDs can happen when the applied voltage is near zero.
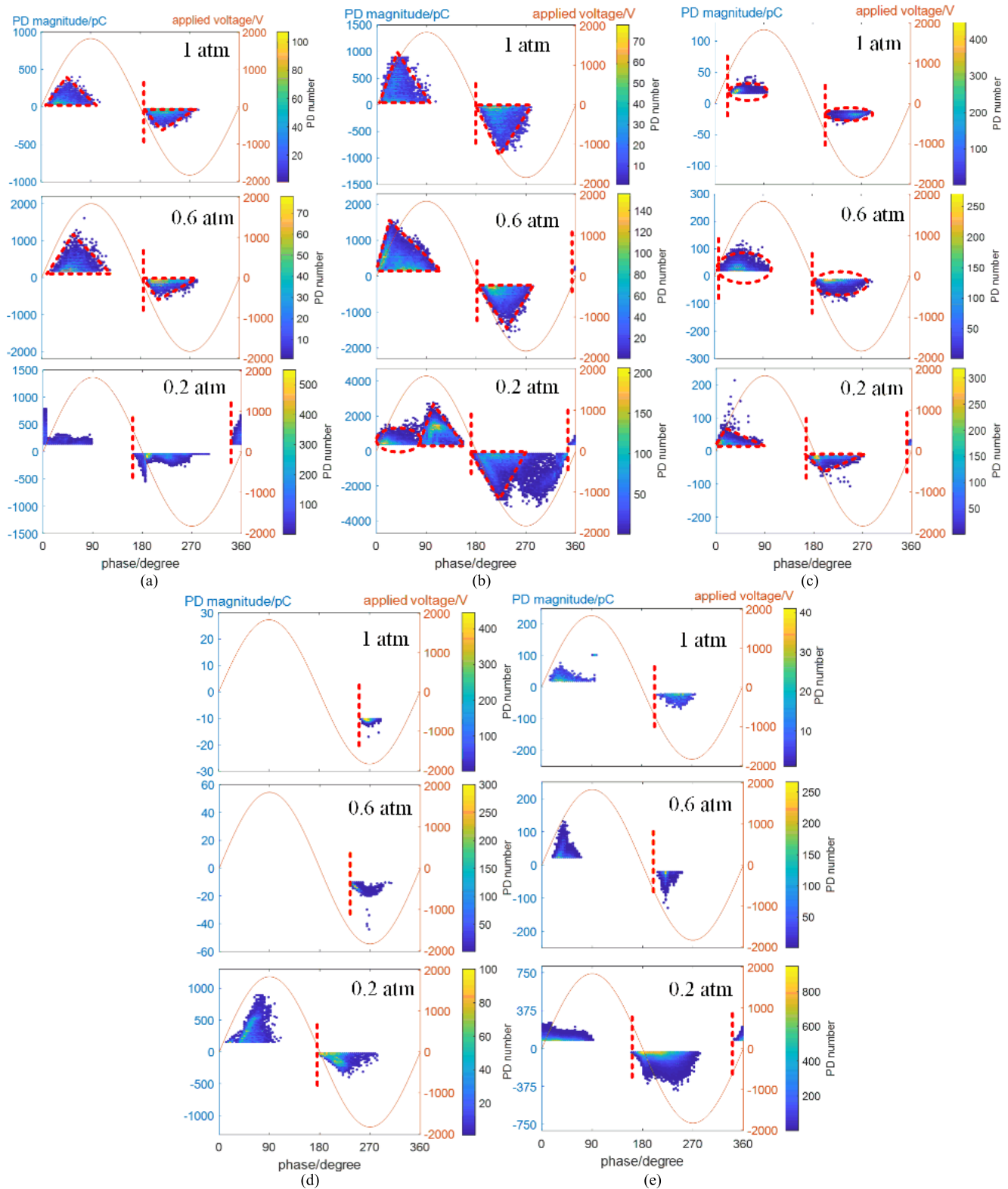
Fig. 8. PRPD patterns of the defect samples and the normal winding at various pressures. (a) Delamination defect at 1, 0.6, and 0.2 atm. (b) Surface defect at 1, 0.6, and 0.2 atm. (c) Void defect at 1, 0.6, and 0.2 atm. (d) Corona defect at 1, 0.6, and 0.2 atm. (e) Normal winding at 1, 0.6, and 0.2 atm.

It is found that the PRPD patterns at low air pressures are different from that of 1 atm, which means that the PD patterns obtained from 1 atm may not be applicable to pattern recognition for low air pressures. It is necessary to extract features that can depict the PD phase and magnitude distribution at low air pressures and thus being utilized for PD pattern recognition. In order to quantitatively compare these PRPD patterns and extract their features at 0.2 atm

TABLE II
STATISTICAL PARAMETERS OF PD PHASE AND MAGNITUDE DISTRIBUTION OF THE WINDINGS AT 0.2 Atm

Parameter	Item	Cycle	Sample type				
			Delamination	Surface	Void	Corona	Winding
Mean value	Magnitude /pC	Positive	285.73	869.03	31.27	389.55	418.07
		Negative	104.43	762.48	26.06	114.68	344.58
	Phase/°	Positive	14.61	64.82	22.83	59.29	27.21
		Negative	212.06	231.99	205.20	213.57	213.44
Skewness	Magnitude/-	Positive	1.27	0.83	3.71	1.34	1.94
		Negative	2.14	1.35	2.83	1.18	2.08
	Phase/-	Positive	1.30	-0.10	0.92	-0.03	0.51
		Negative	0.58	0.81	0.76	0.55	0.18
Kurtosis	Magnitude/-	Positive	4.62	3.61	8.01	6.85	8.21
		Negative	9.03	5.12	7.69	5.26	9.23
	Phase/-	Positive	3.61	3.89	4.30	3.98	2.38
		Negative	2.61	5.68	2.73	6.94	2.20

(cruising altitude for aircraft), statistical parameters are utilized to depict the profile of these discrete distributions. Apparently, the PRPD patterns in each figure can be roughly divided into two parts based on the occurrence phase angle. Approximately, one cluster is located between 0° and 180° and the other between 180° and 360°, which are called the positive and negative half cycle, respectively. The phase and magnitude distribution of all four defect samples and the normal winding are analyzed by statistical parameters, such as mean value, variance, skewness, and kurtosis as follows:

$$\mu = \frac{1}{N} \sum_{i=1}^{N} y_i \qquad (2)$$

$$\sigma^2 = \frac{1}{N} \sum_{i=1}^{N} (y_i - \mu)^2 \qquad (3)$$

$$S_k = \frac{1}{\sigma^3 N} \sum_{i=1}^{N} (y_i - \mu)^3 \qquad (4)$$

$$K_u = \frac{1}{\sigma^4 N} \sum_{i=1}^{N} (y_i - \mu)^4 \qquad (5)$$

where μ is the mean value, N is the number of the PD phase data or magnitude data of positive or negative half cycle, y_i is the PD phase or magnitude of the positive or negative half cycle, σ^2 is the variance, S_k is the skewness, and K_u is the kurtosis. If the distribution is symmetric, $S_k = 0$; if it is asymmetric to the left, $S_k > 0$; and asymmetric to the right, $S_k < 0$. For $K_u = 3$, the distribution has the same sharpness as a normal distribution. If it is sharper than normal, $K_u > 3$, and flatter, $K_u < 3$. The mean value, skewness, and kurtosis of the four defect samples and the normal winding at 0.2 atm are shown in Table II.

For the delamination sample, PRPD pattern is characterized by a sharp slope at the onset of the positive and negative half cycle at 0.2 atm. The PD pattern of the surface sample is characterized by the largest PD magnitude among all the defects, which is shown by the mean value of PD magnitude shown in Table II. PD pattern of the positive half cycle is like a combination of a round pack and a triangle pack, while the negative is like two neighboring triangles at 0.2 atm. The wide phase distribution is also a feature of surface PRPD

pattern, which is indicated by the largest mean value of PD phase shown in Table II. The PRPD patterns of void and corona samples both show triangular shape at 02 atm, but the mean positive PD magnitude is much higher than the negative for corona sample. The mean phase of corona PRPD pattern is larger than that of the void sample, showing the difference of phase distribution between void and corona sample. The PRPD pattern of the normal winding at 0.2 atm is not similar to the pattern of any defect sample, indicating that the winding may contain more than one defect, all of them contributing to the change of the PD pattern. Due to the limited length of this article, the topic of how to identify the contribution of each defect type will be presented in future papers. To sum up, the PRPDs of various defects have different features, the statistical parameters can be calculated from PRPD patterns and they can help discriminate the PD source and possible location.

C. Accelerated Aging and Failure Precursor

Since the stator will experience high temperature and low air pressure when used for electric aircraft propulsion, a failure precursor, which can effectively show the insulation condition is essential for the health management of the electric machine. The normal windings were subjected to various ac voltage from 2200 to 2800 V_{rms} at 240 °C and 0.2 atm to accelerate aging until breakdown happens. It should be noted that the aging speed is quite high with these aging parameters, because we constantly monitor the PD activity and want to achieve great efficiency with acceptable failure time. Five windings were tested for each aging condition. Only one curve for each voltage is shown for simplicity since the other tested samples also show similar trends. The PD profiles of these windings are recorded to investigate PD regularity during the aging process. To extract features that can represent the degradation status of the windings, the PD number, apparent charge, and average PD phase interval in each cycle are calculated

$$Q(t) = \int_0^T |i(t)| dt \qquad (6)$$

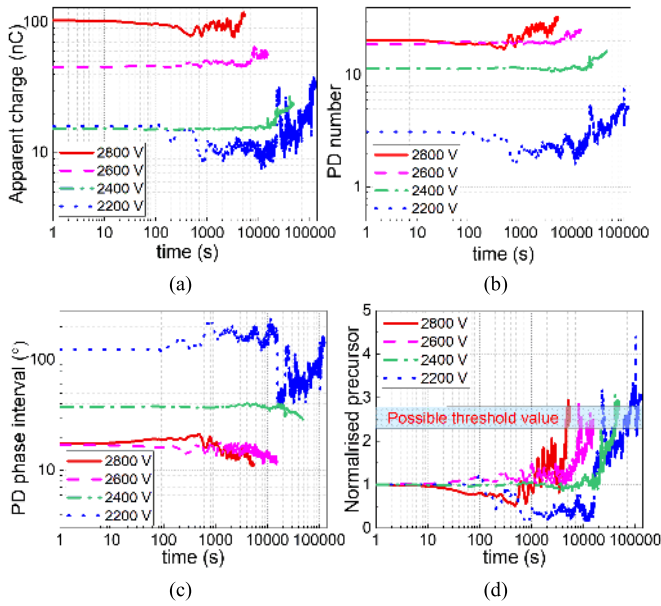$$\Delta p = \frac{1}{N-1} \sum_{i=1}^{N} (p_{i+1} - p_i) \qquad (7)$$

Fig. 9. PD features in accelerated aging at 240 ° 0.2 atm. (a) Apparent charge. (b) PD number. (c) PD phase interval. (d) Normalized precursor.

where Q is the apparent charge, i is the discharge current, T is the period of applied ac voltage, N is the number of PD in one cycle, and p is the PD occurrence phase. To present the trend of these features during aging, the average value of PD number, apparent charge, and PD phase interval in every second of these windings are shown in Fig. 9(a)–(c). It is seen that the PD number and apparent charge generally increase with aging time, whereas PD phase interval decreases. As expected, the PD charge and PD number increase with applied voltage. The time-to-failure also decreases with the increase of applied voltage, indicating the increase of aging speed. Similar results have also been observed by other researchers [29]. The increase of PD number and the decrease of PD interval can be explained by the PD-induced modification of the defects in insulation material and charge transportation process, such as lowering of the injection barrier and/or increase of the surface conductivity, which, respectively, favor electron injection in the defects (such as cavity) and faster decay of the accumulated space charge [29]. With the degradation of insulation, the defect may expand and conductivity could increase due to carbonization. Therefore, the process of charge dissipation accelerates, resulting in more frequent PD occurrence. The increase of apparent charge could be attributed to the acceleration of the physical–chemical conditions of the defects and of the defect-insulation interface [29]. With the degradation of insulation, the accumulated charges increase around the defects. When PD happens, more charges recombine and cause a higher PD magnitude. To comprehensively combine these three different features into one metric that reflects the degree of insulation degradation, a normalized failure precursor is proposed

$$P(t) = \frac{Q(t)N(t)}{p(t)} \bigg/ \frac{Q_0 N_0}{p_0} \qquad (8)$$

where P is the proposed failure precursor. Q, N, and p are the apparent charge, PD number, and PD phase interval at any time during aging; and Q_0, N_0, and p_0 are the apparent charge, PD number, and PD phase interval at the starting moment, respectively. The precursor evolution during the aging process is shown in Fig. 9(d). Although a slight drop can be seen in the early stage, the precursor then increases to more than the starting value before failure. Due to the randomness of the PD phenomenon on time scale, the curves are a little noisy. However, it is feasible to set a threshold value, such as any proper value in the shaded region shown in Fig. 9(d) for this article, to determine whether the motor needs to be stopped and checked preventing from catastrophic failure. To verify the application of the proposed failure precursor to online condition monitoring, more investigations are needed through further online experiments.

Since the proposed failure precursor is related to the PD condition monitoring technique and is supposed to act as an indicator, so that the engineers can rely on this to evaluate the health of winding insulation, it is necessary to review and compare it with current relevant techniques. In terms of the online monitoring methods for the stator insulation system, they can be divided into four categories: temperature monitoring, chemical compounds analysis, vibration monitoring, and electrical signal monitoring. However, the first three categories all have significant drawbacks that limit their applications [30]. Electrical signal monitoring methods are the most widely applied, and continuous attempts have been made to expand available methods and improve accuracy and reliability. Motor-current signature analysis (MCSA) and its variants have been proposed to detect interturn stator fault by obtaining the current spectrum of the motor [31]. However, issues, such as voltage imbalance, and structural imperfections that produce similar effects, are not well addressed. Some researchers have developed high sensitivity differential current transformers to monitor online leakage current and to acquire the capacitance and dissipation factor [32], [33]. They found the three-phase insulation leakage currents and dissipation factor showed a mostly increasing trend during the aging process. However, it should be noted that the dissipation factor trend is indicative of the average condition of the insulation; additional losses due to a single seriously overheated coil in the winding are unlikely to affect the measured value. Thus, whether local defects can be detected by this method is still a question. In recent years, artificial intelligence (AI) methods, such as neural networks, have been proposed to synthesize monitored features and diagnose stator faults [34]. To perform these data-driven methods, a relatively large data set is required to train the AI model. Despite the considerable work that has been done in this area, AI methods are mostly like "black boxes," and much more investigation of their working mechanisms is required to bring such techniques into the mainstream of condition monitoring. The proposed precursor is related to the PD-based metrics, which is widely acknowledged as an early indicator of many electrical faults in machine stators, and the activity is also related to the remaining life of the insulation system. Although the results obtained in this article show the general trend that can give valuable early warning of failure, the application
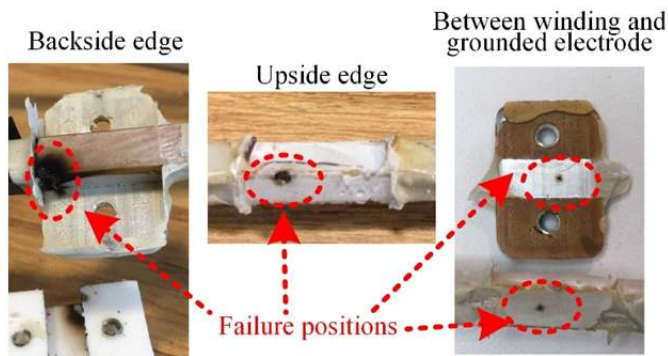
Fig. 10.   Failure positions of the windings aged at 0.2 atm.

of this method for online condition monitoring needs more investigation and will be reported in the future.

During the aging experiment, it is found that the winding can fail in various positions, as shown in Fig. 10. According to electrostatic electric field simulations, the triple point of the copper conductor, the ground electrode, and the air is the position where the electric field is most concentrated. This region is usually covered with enhanced insulation to ensure reliability. However, the breakdown strength of air decreases under the low-pressure situation. Therefore, some locations, such as the backside edge of the winding, that do not cause PD under normal pressure may discharge at low air pressure and could lead to failure. This phenomenon shows that every exposed area or area with less electric field concentration is also dangerous at low air pressures and even the positions with long distance to the ground core iron are possible to cause failure. When designing the insulation structure, these positions can be covered with thermally conductive and high electrically resistive resin to simultaneously mitigate thermal and electrical stress.

V. CONCLUSION

The operation condition, such as low air pressure and high working temperature of the electric machine for electric aircraft propulsion, will pose huge challenges to the stator insulation reliability. To face this, PD characteristics, such as PDIV, PD pattern recognition, and insulation failure precursor, are discussed in this article.

1) It is found that PDIV dramatically decreases and PD magnitude generally increases with the drop of pressure, which can be explained by Paschen's law. This change also results in the PD inception phase shifting to the left as the pressure decreases. It is suggested that a 50%–60% margin should be considered in designing the stator insulation for aircraft propulsion when given the PDIV data at the normal pressure.

2) The PD magnitude and phase distribution changes with pressure. Therefore, the PD patterns obtained from 1 atm may not be applicable to pattern recognition for low air pressures. According to the PRPD results and statistical analysis, delamination, surface, void, and corona defects have different characteristics, so that they can be

discriminated by PD pattern recognition based on these characteristics.

3) According to the simultaneous electrical and thermal accelerated aging experiment, a failure precursor combining the PD apparent charge, number, and phase interval is proposed to monitor the insulating condition. A proper threshold value based on accelerated aging results is feasible to be treated as an alert level for the online PD condition monitoring. For the insulation structure design, it is suggested that the winding edges with long distance to the ground core iron should also be covered with insulation material.

This article focuses on the PD characteristics of form-wound air-core armature windings for electric aircraft propulsion. The experiment results and discussion may provide useful suggestions for the insulation design of the stator winding, defect discrimination based on PD pattern recognition, and failure precursor for the condition monitoring system.

REFERENCES

[1] M.-C. Flynn, C. E. Jones, P. J. Norman, and G. M. Burt, "A fault management-oriented early-design framework for electrical propulsion aircraft," *IEEE Trans. Transp. Electrific.*, vol. 5, no. 2, pp. 465–478, Jun. 2019.

[2] V. Madonna, P. Giangrande, and M. Galea, "Electrical power generation in aircraft: Review, challenges, and opportunities," *IEEE Trans. Transp. Electrific.*, vol. 4, no. 3, pp. 646–659, Sep. 2018.

[3] B. Sarlioglu and C. T. Morris, "More electric aircraft: Review, challenges, and opportunities for commercial transport aircraft," *IEEE Trans. Transp. Electrific.*, vol. 1, no. 1, pp. 54–64, Jun. 2015.

[4] P. Arumugam *et al.*, "High-speed solid rotor permanent magnet machines: Concept and design," *IEEE Trans. Transp. Electrific.*, vol. 2, no. 3, pp. 391–400, Sep. 2016.

[5] American Vacuum Society. (2013). *Atmospheric Pressure at Different Altitudes*. [Online]. Available: https://avs.org/AVS/files/c7/c7edaedb-95b2-438f-adfb-36de54f87b9e.pdf.

[6] P. Neti and B. Wilhelm. *Online Health Monitoring of Motor Insulation*. General Electric Company. Accessed: 2013. [Online]. Available: https:// dme.bz/system/files/products/docs/motor_insulation_health_monitoring_ white_paper_english.pdf

[7] T. Billard, T. Lebey, and F. Fresnet, "Partial discharge in electric motor fed by a PWM inverter: Off-line and on-line detection," *IEEE Trans. Dielectr. Electr. Insul.*, vol. 21, no. 3, pp. 1235–1242, Jun. 2014.

[8] G. C. Montanari and P. Seri, "A partial discharge–based health index for rotating machine condition evaluation," *IEEE Elect. Insul. Mag.*, vol. 34, no. 2, pp. 17–23, Mar. 2018.

[9] L. A. Renforth, R. Armstrong, D. Clark, S. Goodfellow, and P. S. Hamer, "High-voltage rotating machines: A new technique for remote partial discharge monitoring of the stator insulation condition," *IEEE Ind. Appl. Mag.*, vol. 20, no. 6, pp. 79–89, Nov. 2014.

[10] A. Kheirmand, M. Leijon, and S. M. Gubanski, "Advances in online monitoring and localization of partial discharges in large rotating machines," *IEEE Trans. Energy Convers.*, vol. 19, no. 1, pp. 53–59, Mar. 2004.

[11] I. Christou and I. Cotton, "Methods for partial discharge testing of aerospace cables," in *Proc. IEEE Int. Symp. Electr. Insul.*, San Diego, CA, USA, Jun. 2010, pp. 1–5.

[12] R. Rui and I. Cotton, "Impact of low pressure aerospace environment on machine winding insulation," in *Proc. IEEE Int. Symp. Electr. Insul.*, San Diego, CA, USA, Jun. 2010, pp. 1–5.

[13] E. Sili, J. P. Cambronne, N. Naude, and R. Khazaka, "Polyimide lifetime under partial discharge aging: Effects of temperature, pressure and humidity," *IEEE Trans. Dielectrics Electr. Insul.*, vol. 20, no. 2, pp. 435–442, Apr. 2013.

[14] A. Yoon, X. Yi, J. Martin, Y. Chen, and K. Haran, "A high-speed, high-frequency, air-core PM machine for aircraft application," in *Proc. IEEE Power Energy Conf. Illinois (PECI)*, Urbana, IL, USA, Feb. 2016, pp. 1–4.

[15] J. D. Lenz, N. J. Renner, X. Yi, and K. S. Haran, "Insulation considerations in form-wound armature windings for high-frequency electric machines," in *Proc. IEEE Power Energy Soc. Gen. Meeting (PESGM)*, Portland, OR, USA, Aug. 2018, pp. 1–5.

[16] X. Yi, A. Yoon, and K. S. Haran, "Multi-physics optimization for high-frequency air-core permanent-magnet motor of aircraft application," in *Proc. IEEE Int. Electric Mach. Drives Conf. (IEMDC)*, Miami, FL, USA, May 2017, pp. 1–8.

[17] P. Tavner, L. Ran, J. Penman, and H. Sedding, *Condition Monitoring of Rotating Electrical Machines*. London, U.K.: IET, 2008.

[18] G. C. Stone, I. Culbert, E. A. Boulter and H. Duirani, *Electrical Insulation for Rotating Machines: Design, Evaluation, Aging, Testing, and Repair*. Hoboken, NJ, USA: Wiley, 2004.

[19] *Off-Line Partial Discharge Measurements on the Winding Insulation*, Standards IEC 60034-27-1:2017, 2017.

[20] *On-line Partial Discharge Measurements on the stator winding insulation of rotating electrical machines*, IEC standards 60034-27-2:2017, 2017.

[21] A. Rodrigo, P. Llovera, V. Fuster, and A. Quijano, "Influence of high frequency current transformers bandwidth on charge evaluation in partial discharge measurements," *IEEE Trans. Dielectrics Electr. Insul.*, vol. 18, no. 5, pp. 1798–1802, Oct. 2011.

[22] C. B. Barth *et al.*, "Design and control of a GaN-based, 13-level, flying capacitor multilevel inverter," *IEEE J. Emerg. Sel. Topics Power Electron.*, Trondheim, Norway, Nov. 2019, p. 1.

[23] *Functional Evaluation of Insulation Systems—Test Procedures for Form-Wound Windings —Multifactor Evaluation by Endurance Under Simultaneous Thermal and Electrical Stresses*, IEC Standards 60034-18-33:2010, 2010.

[24] *Partial Discharge Resistant Electrical Insulation Systems (Type II) Used in Rotating Electrical Machines Fed From Voltage Converters— Qualification Tests*, IEC Standards 60034-18-42:201, 2017.

[25] M. A. Lieberman, and A. J. Lichtenberg, *Principles of Plasma Discharges and Materials Processing*. New York, NY, USA: Wiley, 2005.

[26] H. A. Toliyat, S. Nandi, S. Choi, and H. Meshgin-Kelk, *Electric Machines: Modeling, Condition Monitoring, and Fault Diagnosis*. New York, NY, USA: CRC press, 2012.

[27] G. Altamimi, H. A. Illias, N. Mokhtar, H. Mokhlis, and A. H. A. Bakar, "Corona discharges under various types of electrodes," in *Proc. IEEE Int. Conf. Power Energy (PECon)*, Kuching, Malaysia, Dec. 2014, pp. 5–8.

[28] H. Illias, T. Soon Yuan, A. H. A. Bakar, H. Mokhlis, G. Chen, and P. L. Lewin, "Partial discharge patterns in high voltage insulation," in *Proc. IEEE Int. Conf. Power Energy (PECon)*, Kota Kinabalu, Malaysia, Dec. 2012, pp. 750–755.

[29] L. Wang, L. Testa, A. Cavallini, and G. C. Montanari, "Relation between the trend of partial discharges and aging models under AC voltage," in *Proc. IEEE 9th Int. Conf. Properties Appl. Dielectric Mater.*, Harbin, China, Jul. 2009, pp. 268–271.

[30] M. F. Cabanas *et al.*, "Detection of stator winding insulation failures: On-line and off-line tests," in *Proc. IEEE Workshop Electr. Mach. Design, Control Diagnosis (WEMDCD)*, Paris, Mar. 2013, pp. 210–219.

[31] T. Yang, H. Pen, Z. Wang, and C. S. Chang, "Feature knowledge based fault detection of induction motors through the analysis of stator current data," *IEEE Trans. Instrum. Meas.*, vol. 65, no. 3, pp. 549–558, Mar. 2016.

[32] P. Neti, K. Younsi, and M. R. Shah, "A novel high sensitivity differential current transformer for online health monitoring of industrial motor ground-wall insulation," in *Proc. IEEE Energy Convers. Congr. Expo.*, Denver, CO, USA, Sep. 2013, pp. 2493–2499.

[33] J. Yang, J. Cho, S. B. Lee, J.-Y. Yoo, and H. D. Kim, "An advanced stator winding insulation quality assessment technique for inverter-fed machines," *IEEE Trans. Ind. Appl.*, vol. 44, no. 2, pp. 555–564, Mar./Apr. 2008.

[34] R. C. Bhavsar, R. A. Patel, and B. R. Bhalja, "Condition monitoring of induction motor using artificial neural network," in *Proc. Annu. Int. Conf. Emerg. Res. Areas, Magn., Mach. Drives (AICERA/iCMMD)*, Kottayam, Kerala, Jul. 2014, pp. 1–6.
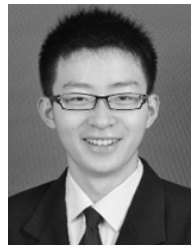
Yalin Wang (Member, IEEE) was born in Anhui, China, in 1992. He received the B.Eng. degree from Xi'an Jiao Tong University, Shaanxi, China, in 2014, and the Ph.D. degree from Shanghai Jiao Tong University, Shanghai, in 2018.

He is currently a Post-Doctoral Researcher with Shanghai Jiao Tong University and a Visiting Scholar with the University of Illinois Urbana-Champaign, Urbana, IL, USA. His research interests include dielectric properties of insulation materials and condition monitoring.

Thanatheepan Balachandran was born in Sri Lanka. He received the B.SC. degree from the University of Peradeniya, Sri Lanka, in 2013, and the M.Sc. degree from Wichita State University, Wichita, KS, USA, in 2017. He is currently pursuing the Ph.D. degree with the University of Illinois Urbana-Champaign, Urbana, IL, USA.

His research interests include electrical machines and drives, electric propulsion, and superconducting machines.

Yovahn Hoole was born in Colombo, Sri Lanka, in 1997. He received the B.S. degree in computer science and electrical engineering from Rice University, Houston, TX, USA, in 2018. He is currently pursuing the M.Sc. degree in electrical engineering with the University of Illinois Urbana-Champaign, Urbana, IL, USA.

His current research focuses on the use of sensors and data driven models to accurately diagnose, control, and predict the faults of electric machines in real time.

Yi Yin (Member, IEEE) was born in Jiangsu, China. He received the M.Eng. and Ph.D. degrees in electrical engineering from Xi'an Jiao Tong University, Xi'an, China, in 1997 and 2000, respectively.

He is currently a Professor with the Department of Electrical Engineering, School of Electronic Information and Electrical Engineering, Shanghai Jiao Tong University, Shanghai, China. His main research interests are dielectric properties of polymer composites, high-voltage technology, condition monitoring, and diagnosis.

Kiruba Sivasubramaniam Haran (Fellow, IEEE) received the Ph.D. degree in electric power engineering from Rensselaer Polytechnic Institute, Troy, NY, USA, in 2000.

He spent 13 years as a Senior Engineer and the Manager of the Electrical Machines Laboratory, GE Research Center, Niskayuna, NY, USA. In 2014, he moved to the University of Illinois Urbana-Champaign, Urbana, IL, USA, to join the Grainger Center for Electric Machinery and Electromechanics and the Faculty of Electrical and Computer Engineering.